# Plasma Electrodynamics and Applications

**Academic and Research Staff**
Professor Abraham Bers, Dr. Abhay K. Ram

**Visiting Scientists and Research Affiliates**
Prof. Alain Brizard (St. Michael's College, Colchester, Vermont), Dr. Ronald J. Focia (Kulicke & Soffa Industries, Inc., Willow Grove, Pennsylvania), Dr. Chris N. Lashmore-Davies (EURATOM, United Kingdom Atomic Energy Authority, Culham Science Centre, Abingdon, Oxfordshire, U.K.), Dr. Yves Peysson (TORE-SUPRA, Commissariat à l'Énergie Atomique, Cadarache, France), Dr. Ante Salcedo (McKinsey & Company, Inc., Mexico City, Mexico)

**Graduate Students**
Joan Decker, Brian C. Ross, David J. Strozzi

**Technical and Support Staff**
Laura M. von Bosau

## Introduction

The work of this group is concerned with phenomena relevant to controlled fusion energy generation in high-temperature plasmas that are confined magnetically or inertially, and phenomena in space plasmas. We report on four studies of the past year.

Sections 1 and 2 report new results that clarify the two possible heating and current drive mechanisms using electron cyclotron waves in toroidally confined, high-temperature plasmas. This work makes use of the newly developed DKE code – a relativistic code that solves the 2-D (in momentum space) drift kinetic equation, including Fokker-Planck operators for collisions and quasi-linear diffusion due to wave fields – described in last year's progress report.[1] The Ohkawa mechanism for driving current is analyzed in detail in 2-D momentum space, for the first time, and shown to be of importance in advanced tokamak operation scenarios.

Section 3 reports results from our continuing study[2] of the nonlinear ion energization by two electrostatic waves propagating obliquely to the plasma confining magnetic field. Detailed scalings with frequencies, wavenumber differences and amplitudes have been established and a paper prepared for journal publication. The result should be useful to ongoing experiments (at Princeton University, with Prof. Edgar Choueiri) aimed at observing this mechanism (first proposed by us), and for possible use in deep space propulsion. The studied mechanism may also be useful in understanding certain observed ion energizations in the upper ionosphere toward the magnetosphere, and possibly as new means for ion heating in fusion plasmas.

Section 4 reports progress on our study[3] of ion energization in very localized fields as are observed in density cavities in the upper ionosphere.

---

[1] J. Decker, Y. Peysson, A. Bers, and A. K. Ram, "Plasma Electrodynamics and Applications: Section 3 – New Code and Results on LHCD and ECCD Synergism With the Bootstrap Current," *Progress Report No. 144,* MIT Research Laboratory of Electronics, Cambridge, 2002, Chapter 16, pp. 23–27 (http://rleweb.mit.edu/Publications/pr144/default.htm).

[2] D. Strozzi, A. K. Ram, and A. Bers, "Plasma Electrodynamics and Applications: Section 4 – Chaotic Dynamics in Two Electrostatic Waves Propagating Obliquely to $\vec{B}$," *Progress Report No. 144,* MIT Research Laboratory of Electronics, Cambridge, 2002, Chapter 16, pp. 28–32 (http://rleweb.mit.edu/Publications/pr144/default.htm).

[3] A. K. Ram and A. Bers, "Plasma Electrodynamics and Applications: Section 5 – Energization of Ions by Spatially Localized Fields," *Progress Report No. 144,* MIT Research Laboratory of Electronics, Cambridge, 2002, Chapter 16, pp. 33–36 (http://rleweb.mit.edu/Publications/pr144/default.htm).

## 1. Ohkawa Versus Fisch-Boozer Method for Driving Current With Electron Cyclotron Waves

**Sponsors**
Department of Energy (DoE) Contract DE-FG02-91ER-54109

**Project Staff**
J. Decker, Professor A. Bers, Dr. A. K. Ram, and Dr. Y. Peysson

Electron Cyclotron Waves (ECW) are of importance in tokamaks for both heating and current drive. They are particularly attractive because it is possible to accurately control (by steering mirrors) and predict their propagation and the location of the interaction, at the intersection of the ray path and the Doppler-shifted cyclotron resonance layer. ECW are therefore the main candidate when a localized, predictable and controllable source of current or heat is needed, such as for sustaining steady-state shear profiles,[4] or stabilizing neoclassical tearing modes (NTM).[5] There are two methods for driving current using ECW: the usual Fisch-Boozer method[6] (ECCD), and also the Ohkawa method[7] (referred to as OKCD). The latter has not been used experimentally but may become a good alternative, as current drive is increasingly needed off-axis in advanced tokamak operations. The mechanisms of both ECCD and OKCD will be presented in Section A, and studied in more details in Section B using the kinetic DKE code.[8,9] A quantitative comparison between ECCD and OKCD in Section C will show that, depending on the plasma and ECW parameters, one or the other method will be more appropriate.

### *A. Brief Description of the Physical Mechanisms of ECCD and OKCD*

Electrons can interact with an ECW — of frequency $\omega$ and parallel wave number $k_{\|}$ — only if the component of their velocity parallel to the magnetic field, $V_{\|}$, satisfies the resonance condition

$$\omega - k_{\|} V_{\|} - n\Omega = 0 \tag{1}$$

[4] O. Sauter, M. A. Henderson, F. Hofmann, T. Goodman, S. Alberti, C. Angioni, K. Appert, R. Behn, P. Blanchard, P. Bosshard, R. Chavan, S. Coda, B. P. Duval, D. Fasel, A. Favre, I. Fumo, P. Gorgerat, J. P. Hogge, P. F. Isoz, B. Joye, P. Lavanchy, J. B. Lister, X. Llobet, J. C. Magnin, P. Mandrin, A. Manini, B. Marletaz, P. Marmillod, Y. Martin, J. M. Mayor, A. A. Martynov, J. Mlynar, J. M. Moret, C. Nieswand, P. Nikkola, P. Paris, A. Perez, Z. A. Pietrzyk, R. A. Pitts, A. Pochelon, G. Pochon, A. Refke, H. Reimerdes, J. Rommers, E. Scavino, G. Tonetti, M. Q. Tran, F. Troyon, and H. Weisden, "Steady-State-Fully Noninductive Current Driven by Electron Cyclotron Waves in a Magnetically Confined Plasma," *Phys. Rev. Lett.* 84(15): 3322-25 (2000).

[5] R. J. La Haye, S. Gunter, D. A. Humphreys, J. Lohr, T. C. Luce, M. E. Maraschek, C. C. Petty, R. Prater, J. T. Scoville, and E. J. Strait, "Control of Neoclassical Tearing Modes in DIII-D," *Phys. Plasmas* 9(5): 2051-60 (2002).

[6] N. J. Fisch and A. H. Boozer, "Creating an Asymmetric Plasma Resistivity With Waves," *Phys. Rev. Lett.* 45(9): 720-22 (1980).

[7] T. Ohkawa, "Steady State Operation of Tokamaks by RF Heating," *General Atomics Company Report No.* GA-A13847 (1976).

[8] J. Decker, Y. Peysson, A. Bers, and A. K. Ram, "Plasma Electrodynamics and Applications: Section 2 – Self-Consistent Calculation of ECCD and OKCD With the Bootstrap Current," *Progress Report No. 145,* MIT Research Laboratory of Electronics, Cambridge, 2002.

[9] J. Decker, Y.Peysson, A. Bers, and A. K. Ram, "Self-Consistent ECCD Calculations With Bootstrap Current," *Proc. 12th Joint Workshop on Electron Cyclotron Emission and Electron Cyclotron Resonance Heating,* Aix-en-Provence, France, May 13–16, 2002, to be published by World Scientific (Singapore), pp. 113–118, also (http://wshop.free.fr/ec12/PAPERS/084-Peysson.pdf).

for some harmonic $n$ of the cyclotron frequency $\Omega = eB/m$. Therefore, it is possible, by controlling the parallel wave number, to choose what parallel velocity the interacting electrons will have. The interaction between electrons and ECW can be described kinetically quite accurately as a quasi-linear diffusion in velocity space. The diffusion is mostly directed in perpendicular velocity, except for very relativistic electrons. The main effect of ECW is to heat the electrons. However, asymmetric heating, obtained by

launching a wave with an asymmetric $k_{\parallel}$ spectrum, can generate a current, through at least two different processes, which have opposing effects.

The first effect is referred to as the Fisch-Boozer effect, and results from an induced asymmetry in the electron collisional resistivity: if only electrons with a negative parallel velocity are heated ($k_{\parallel}<0$), their collisional resistivity is lower compared to electrons with a positive parallel velocity. Therefore, the slowing down due to collisions will affect primarily electrons with a positive velocity, resulting in a negative parallel electron flow; since electrons carry a negative charge, a positive current is generated. This is the usual effect referred to for driving current with ECW, and this method is denoted ECCD.

The second effect has been first described by Ohkawa[7] and relies on the presence of magnetically trapped electrons in the equilibrium distribution function. If the wave-particle interaction region in velocity space is located near the trapped/passing boundary, a significant trapping can be induced by the quasilinear (QL) diffusion due to the EC waves. If the interaction affects only electrons with a positive velocity ($k_{\parallel}>0$), an asymmetric trapping is induced. Since the detrapping is symmetric with respect to $V_{\parallel}$, a net parallel electron flow is created in the negative direction, which in turn generates a positive current. We refer to this method as OKCD.

These two methods for driving a parallel current using ECW are shown schematically on Figure 1. In most tokamak configurations, both collisions and electron trapping have to be considered. Consequently, any current drive scheme with ECW will result from the relative importance of the opposing Fisch-Boozer and Ohkawa effects. Whether the Fisch-Boozer method (ECCD), or the Ohkawa method (OKCD), should be used must be related to the plasma and wave parameters.

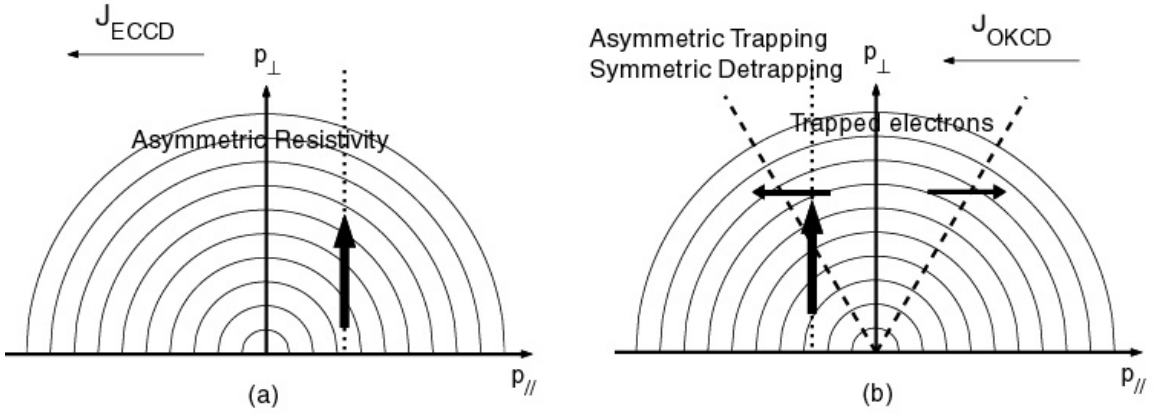


**Figure 1**: Schematic Description of the (a) ECCD and (b) OKCD Methods in electron momentum space. Contours indicate constant levels of the unperturbed distribution function. The QL diffusion in momentum space due to EC waves is represented by thick arrows.

### *B. Detailed Kinetic Mechanism Using the DKE Code*

The DKE Code[8,9] can be used to solve the steady-state bounce-averaged Quaslinear (QL) Fokker-Planck (FP) Equation $\{C(f)\} + \{Q(f)\} = 0$. This is a 2-D equation in momentum space, which accounts for collisions and QL diffusion induced by radio frequency (RF) waves including ECW. In addition, this code has an implicit treatment of the particle fluxes between the trapped and passing regions in momentum space, which allows for a fast and accurate convergence to the steady-state distribution function. Both Fisch-Boozer and Ohkawa effect can therefore be described using the DKE code. The validity of this treatment

is confined to low collisionality regimes, to which we restrict ourselves from now on. Only second harmonic X-mode ECCD and OKCD will be considered here, as it concerns most experimental situations.

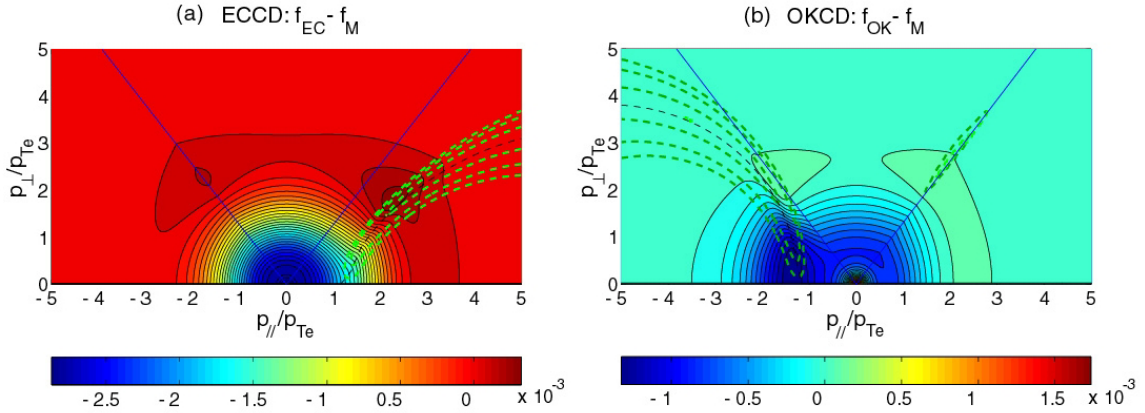


**Figure 2**: Momentum space variations in the distribution function due to (a) ECCD and (b) OKCD. Green dashed lines are contour plots of the diffusion coefficient.

On Figure 2 are displayed the steady-state distribution function for the cases of ECCD and OKCD, from which the unperturbed Maxwellian was removed for clarity. The cases presented here are computed with Alcator C-Mod parameters[10] at *r/a=0.7*, a local wave power of $P_{EC}$=10 MW, and wave parameters that correspond to the optimized respective configurations for ECCD ($N_{//}$=-0.30, $2\Omega/\omega$=0.98, $\theta$=180°) and OKCD ($N_{//}$=-0.30, $2\Omega/\omega$=0.98, $\theta$=0°), as explained in Section C. The green dashed lines are contour plots of the diffusion coefficient, and therefore represent the region where wave-particle interaction occurs. The diffusion is directed mostly perpendicularly.

The Fisch-Boozer effect can be associated with the accumulation of electrons at high $p_\parallel$ and high $p_\perp$, which are very energetic, present a low collisionality and drive a large current, as it is seen on graph (a) (ECCD). However an enhanced pitch-angle scattering, due to the "short-circuit" effect of the trapped region, results in an accumulation of particles with negative $p_\parallel$, which reduces the amount of driven current. This effect occurs even if there is no trapped electron in the resonance region ($\theta$=180°).

The Ohkawa effect appears as a "sink" of electrons with negative $p_\parallel$ just under the trapped/passing boundary, visible on graph (b) (OKCD). These electrons are trapped due to the action of the wave (increased $p_\perp$ due to QL diffusion, leading to trapping), with a symmetric detrapping. This sink creates a net electron flow in the opposite (positive) direction. It is worth noting that OKCD is optimized when the resonance region in momentum space is located right under the trapped/passing boundary, so as to obtain the maximum wave-induced trapping.

### *C. Quantitative Study of ECCD and OKCD in a Tokamak Configuration*

We consider the issue of driving a parallel current on a given flux surface. For simplicity, the magnetic flux surfaces are assumed to be circular and concentric, so that a given flux-surface is parametrized by its normalized radius $\rho$=*r/a*. The fraction of trapped electrons vanishes towards the toroidal axis, so that the only method for central current drive is ECCD. We therefore focus here on off-axis current drive, where OKCD may be a valuable alternative to ECCD.

OKCD is based on wave induced trapping of electrons, and therefore must be optimum where the fraction of trapped particles is maximum, that is, on the outboard (low field) side (poloidal angle $\theta$=0°). On the other hand, trapped particles have a negative effect in the ECCD configuration, so that ECCD must be set

[10] P. T. Bonoli, R. R. Parker, M. Porkolab, J. J. Ramos, S. J. Wukitch, Y. Takase, S. Bernabei, J. C. Hosea, G. Schilling, and J. R. Wilson, "Modelling of Advanced Tokamak Scenarios With LHCD in Alcator C-Mod," *Nuclear Fusion*, 40(6):1251-56 (2000).

up where the fraction of trapped particle is lowest, on the inboard (high field) side ($\theta$=180°). The present study will be limited to these two optimum configurations.

The diffusion in momentum space is characterized by a QL diffusion coefficient $D_{QL}(\boldsymbol{p})$, whose profile in $\boldsymbol{p}$ –space is primarily determined by the power spectrum $P_{EC}(k_{\parallel})$ and the resonance condition (1). For a narrow profile centered around a central wave number $k_{\parallel 0}$, the diffusion region closely follows an ellipse in $\boldsymbol{p}$ –space which is parametrized by the dimensionless cyclotron frequency $y=n\Omega/\omega$ and the dimensionless wave number $N_{\parallel}=k_{\parallel 0}c/\omega$. $N_{\parallel}$ is determined by the ECW launching set up and typically does not vary significantly across the resonance layer. However, the parameter $y$ varies rapidly across the resonance region and is strictly equal to 1 on the cyclotron resonance surface. This variation affects greatly the results of ECCD and OKCD.

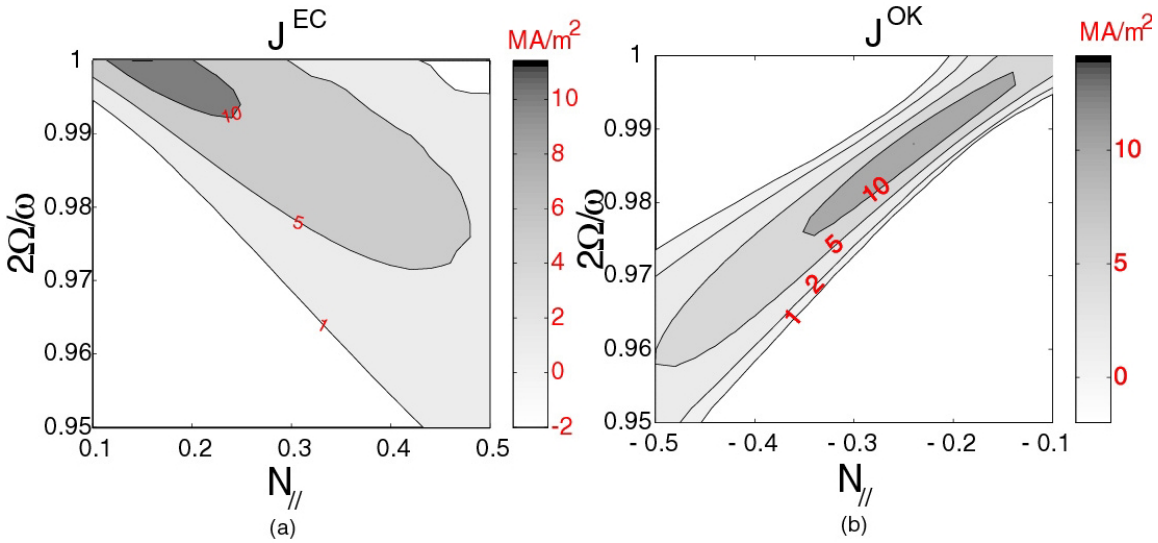


**Figure 3**: Density of (a) EC and (b) OK driven current for Alcator C-Mod parameters, at r/a=0.7, with a normalized diffusion coefficient Dec=0.14 $\nu_e p_{Te}^2$.

The computational results from the DKE code are displayed on Figure 3 where the driven currents are computed respectively for ECCD ($\theta$=180°) and OKCD ($\theta$=0°) for a wide range of wave parameters. Schematically, it can be considered that $N_{\parallel}$ remains roughly constant along the propagation path, while $y$ varies rapidly from 0.95 to 1.05 over a resonance layer whose thickness is typically a few centimeters. For tokamak parameters chosen in the case presented on Figure 3, that is, Alcator C-Mod parameters[10] at $\rho$=0.7 with a normalized diffusion coefficient $D_{EC}$=0.14, it can be noted that the maximum current density that can be driven by ECCD and OKCD are of the same order, while the resulting radial current profile seem to be significantly more narrow for OKCD, which is important when a very localized source of current is called for.

| Method | ECCD | OKCD |
|---|---|---|
| $\rho$=r/a | 0.7 | 0.7 |
| $\theta_b$ | 180° | 0° |
| $\phi_L$ | 8 | -15 |
| $J_{\parallel}$ (kA) | 10.5 | 11.2 |
| $P_{abs}$ (MW) | 1.9 | 2.0 |

Table 1: ECCD and OKCD with Alcator C-Mod parameters

In order to compare ECCD and OKCD on a global scale, it is necessary to compute the total amount of current generated from the damping of a EC beam, which requires the use of some propagation model. Here we use a simple model assuming straight-line propagation, which is a valuable approximation for ECW as long as the resonance region remains far from wave resonances and cut-off surfaces. The launching parameters (including the toroidal steering angle $\phi_L$), which determine the wave path and wave number, are chosen so as to optimize the total current driven, with a profile centered on the surface $\rho$=0.7. The plasma parameters are those of Alcator C-Mod, [10]

with an initial beam power $P_{EC}$=2.0 MW. The parameters and results are summarized in Table 1, and the current and power profiles are shown on Figure 4.

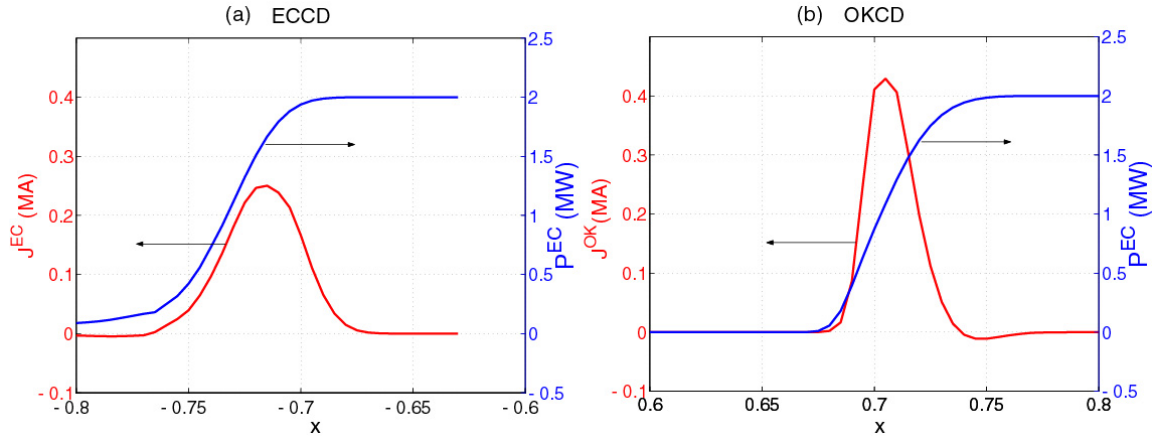


**Figure 4**: Profiles of driven current (J) and remaining power (P) for (a) ECCD and (b) OKCD (right) with parameters in Table 1.

In this particular case, 100% of the ECW power is absorbed in a single pass for OKCD, and 95% for ECCD. The total amount of driven current is of the same order, though a bit higher for OKCD. On the OKCD current profile, we can observe that a small negative current is generated by Fisch-Boozer effect as the wave enters the resonance region. Indeed, at this position, the resonance region in momentum space is still far from the trapped/passing boundary, such that the Fisch-Boozer effect still dominates. It is also interesting to note that the current profile is more narrowly peaked for OKCD as compared to ECCD.

### *D. Conclusions*

The physical mechanism of ECCD and OKCD was described at a kinetic level and illustrated with the code DKE. The EC driven current results from an accumulation of low-resistivity electrons with a positive velocity. This accumulation is created by asymmetric heating through the action of QL diffusion and collisions. OK driven current is the consequence of a flux of electrons through the trapped passing boundary, which creates a sink on the negative passing region.

In most tokamak configurations, there is a threshold (typically $\rho$~0.7 in Alcator C-Mod) in a radial position beyond which OKCD would drive more current than ECCD for a given beam power. The threshold would be even lower ($\rho$~0.5) when OKCD is compared with a ECCD configuration on the main axis ($\theta$=90°), which is often used in experiments. OKCD also presents two additional advantages: First, the wave frequency needed on the low-field side is significantly lower than that needed on the high-field side (180 GHz vs 290 GHz at second harmonic in Alcator C-Mod), which is an important point given the technological challenges of building high frequency, high power sources. Second, OKCD allows one to generate narrower radial current profiles, which can be very useful for highly localized current drive.

## 2. Self-Consistent Calculation of ECCD and OKCD With the Bootstrap Current

**Sponsors**
Department of Energy (DoE) Contract DE-FG02-91ER-54109

**Project Staff**
J. Decker, Dr. Y. Peysson, Professor A. Bers, Dr. A. K. Ram

Advanced scenarios of steady-state operation in tokamaks rely on a large bootstrap-driven fraction of the toroidal current, supplemented by radio-frequency (RF) driven currents. Electron Cyclotron (EC) waves have been successfully used for this purpose, sustaining a steady-state in TCV.[4] However, for transport barrier formation, current drive (CD) is increasingly needed far off axis where the fraction of trapped particles is significant. A consequence of this is that the ECCD efficiency decreases as the current is driven further off-axis, eventually to a point where Ohkawa current drive (OKCD), which uses trapping to generate current, becomes an attractive alternative.[11] In addition, at the location of off-axis ECCD, a large bootstrap current may exist. A strongly non-maxwellian distribution may be sustained by EC waves, which could affect the bootstrap current at a kinetic level. Conversely, the perturbation in the distribution due to radial drifts could affect ECCD or OKCD. Therefore, EC and OK driven currents have to be calculated self-consistently with the bootstrap current (BC). The kinetic model used in our description is presented briefly in Section A. The interaction, at a kinetic level, between ECCD or OKCD and the bootstrap current, is investigated in Section B, using the code DKE. In Section C, a quantitative study of the resulting synergism is reported.

### *A. Self-Consistent Kinetic Description of RFCD and the Bootstrap Current*

A self-consistent description, for axisymmetric plasmas, of the RF driven current with the effect of radial drifts due to the magnetic field gradient and curvature is obtained from the steady-state drift-kinetic equation (DKE)

$$\frac{v_\theta}{r}\frac{\partial f}{\partial \theta} + v_{Dr}\frac{\partial f}{\partial r} = C(f) + Q(f) \tag{2}$$

where $f$ is the electron distribution function, $(r,\theta)$ are the radial and poloidal positions, $v_\theta$ is the velocity along the poloidal field lines and $v_{Dr}$ is the drift velocity across the field lines. The effects of collisions and RF driven quasilinear diffusion are described, respectively, by the relativistic operators $C(f)$[12] and $Q(f)$[13]. The distribution function is expanded as $f \approx f_0 + f_1 = f_0 + \tilde{f} + g$ where the expansion parameter is $\delta = v_{Dr} / v_\theta$. Here $f_0$ is the RF-generated distribution unperturbed by radial drifts and given by the usual bounce-averaged Fokker-Planck (FP) equation in the absence of BC. $\tilde{f}$ is the perturbation due to radial drifts and gradients, and $g$ is the response of the plasma due to collisions and RF fields. In the low-collisionality regime, the collisional detrapping time $\tau_{dt}$ is much longer than the bounce time $\tau_b$ of trapped electrons, so that a sub-ordering $\delta << \tau_b / \tau_{dt} << 1$ can be used to further expand and solve (2):[14]

$$\{C(f_0)\} + \{Q(f_0)\} = 0 \tag{3}$$

---

[11] J. Decker, Y. Peysson, A. Bers, and A. K. Ram, "Plasma Electrodynamics and Applications: Section 1 – Ohkawa Versus Fisch-Boozer Method for Driving Current With Electron Cyclotron Waves," *Progress Report No. 145,* MIT Research Laboratory of Electronics, Cambridge, 2002.
[12] B. J. Braams and C. F. F. Karney, "Conductivity of a Relativistic Plasma," *Phys. Fluids B* 1(7): 1355-68 (1989).
[13] I. Lerche, "Quasilinear Theory of Resonant Diffusion in a Magneto-Active, Relativistic Plasma," *Phys. Fluids* 11(8): 1720-26 (1968).
[14] S. D. Schultz, *Lower Hybrid and Electron Cyclotron Current Drive With Bootstrap Current in Tokamaks,* Ph.D. dissertation, Department of Physics, MIT, September, 1999.

$$\tilde{f} = -\frac{v_{//}}{\Omega_\theta}\frac{\partial f_0}{\partial r} \tag{4}$$

$$\{C(g)\} + \{Q(g)\} = -\{C(\tilde{f})\} - \{Q(\tilde{f})\} \tag{5}$$

where { } denotes the bounce-averaging operation, $v_{//}$ is the particle velocity along the field line, and $\Omega_\theta$ is the poloidal gyrofrequency.

The system (3)–(5) is solved in the small inverse aspect ratio approximation $\epsilon = r/R_0 << 1$, using the 3-D, bounce-averaged, relativistic, quasilinear Fokker-Planck code DKE that calculates the steady-state distribution function $f$ in momentum space at the radial position $r$. Details of the numerical schemes in DKE and its novel treatment of the trapped-passing boundary in momentum space are already given.[1,9]

In order to evaluate the interaction between RF driven currents and the bootstrap current, the following flux surface averaged quantities are computed: $J^{RF}$ and $P^{RF}$, which are, respectively, the RF current density and the density of power absorbed, in the absence of the BC; $J^B$, the BC density in the absence of RF; $J$ and $P$, which are, respectively, the self-consistent total current density and the total density of power absorbed. The synergistic current density is given by $J^S = J-(J^{RF} + J^B)$, and the internal figure of merit for the current drive is given by $\eta = (J - J^B)/P$. This is compared with $J^{RF} / P^{RF} = \eta^{RF}$.

### *B. Mechanisms of the Synergism between ECCD or OKCD and the Bootstrap Current*

In the absence of perturbations due to RF waves, the system (3)–(5) reduces to

$$\tilde{f}_M = -\frac{v_{//}}{\Omega_\theta}\frac{\partial f_M}{\partial r} \tag{6}$$

and

$$\{C(g_M)\} = -\{C(\tilde{f}_M)\} \tag{7}$$

where the zero order distribution is a Maxwellian $f_0 = f_M$. The first order distribution $f_{1M} = \tilde{f}_M + g_M$, due to the presence of radial drifts, determines the bootstrap current $J_B = q_e \int v_{//} f_{1M} d^3p$ .The "bootstrap distribution" $f_{1M}$ is antisymmetric in $p_{//}$, and a contour plot of this distribution in momentum space is shown on Figure 5 for typical Alcator C-Mod parameters[10] at a normalized radius $\rho \equiv r/a = 0.7$.

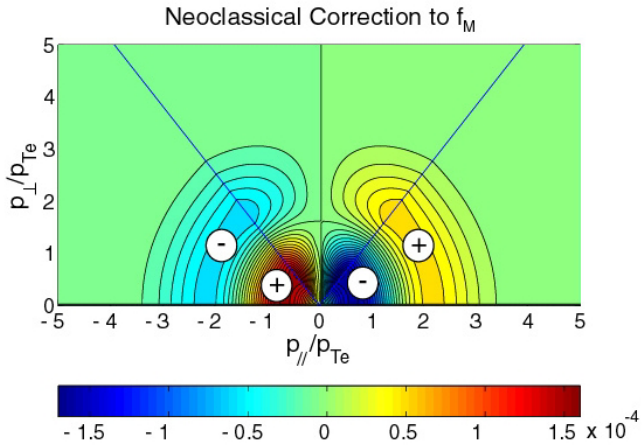


**Figure 5**: Perturbation to the Maxwellian distribution, due to radial drifts. The parallel velocity moment of this first-order distribution gives the bootstrap current. For clarity, the signs of the perturbation in different regions of the momentum space are shown.

The mechanisms of ECCD and OKCD have been described.[11] Solving the full system (3)–(5) gives the total self-consistent calculation of RFCD and the bootstrap current. The difference $f_S = f_1 - f_{1M}$ is the synergistic part of the distribution function, and can be interpreted as the effect of RF waves on the bootstrap distribution, or vice versa.

1) ECCD + BC

We first consider the case of ECCD; the plasma parameters are those of Alcator C-Mod at $\rho$=0.7, and the wave parameters ($N_{//}$=0.30, $2\Omega/\omega$=0.98) are such as to optimize the EC driven current density[11] for an incident power of $P_{EC}$=10 MW. The wave-particle interaction is chosen to be located on the high-field side ($\theta$=180°) so as to maximize the EC driven current.[11] In Figure 6 are displayed contour plots of both $f_1$ and $f_{1M}$, in order to visualize the effect of EC quasilinear diffusion on the bootstrap distribution. The green dashed lines are a contour plot of the EC diffusion coefficient. We do not consider the effect on the inverted central part of the distribution $f_1$ ($p$<1.5$p_{Te}$) as its contribution to the current is negligible.

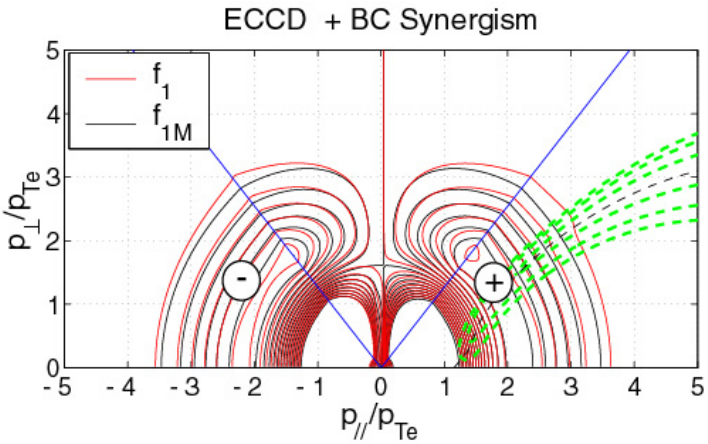


**Figure 6**: Bootstrap distribution unperturbed (black) and perturbed (red) by ECCD. The QL diffusion coefficient is represented by green dashed contours. The black dashed line is the resonance curve.

First, we can observe a Fisch-Boozer effect on $f_{1M}$ resulting in an accumulation of electrons with high $p_{//}$, $p_\perp$, and a deficiency of electrons at lower $p_{//}$, $p_\perp$ , which generates a net positive, synergistic current. This is equivalent to saying that the perturbation due to radial drifts, described by $f_{1M}$, enhances ECCD by bringing more electrons (plus sign on Figure 6) in the region affected by the Fisch-Boozer mechanism. In addition, we recall that the presence of trapped particles has a negative effect on $f_0$ because the trapped region, where $f_0$ is symmetric, acts like a short circuit in pitch-angle scattering. However, since $f_1$ has to be antisymmetric in the trapped region, pitch-angle scattering through the trapped/passing boundary for $p_{//}$>0 contributes to an increase in the magnitude of $f_1$ for $p_{//}$<0. Since $f_1$ is negative there, a positive synergistic current is generated.

The result of enhanced ECCD and antisymmetry in $f_1$ is a net positive, synergistic current. The current densities, and densities of power absorbed, are displayed in Table 2. There is a 7% synergism on the amount of EC driven current. As the power absorbed remains essentially the same, there is a net, 6% increase in the figure of merit.

| ECCD | BC | EC | EC+SYN | SYN |
|---|---|---|---|---|
| $J_{//}$ (MA/m$^2$) | 2.3 | 9.25 | 9.86 | 7% |
| $P_{abs}$ (MW/m$^3$) | - | 194 | 194.4 | 0% |
| $\eta$ (Am/W) | - | 0.0477 | 0.0507 | 6% |

**Table 2**: Results of the ECCD+BC computation for Alcator C-Mod parameters at r/a=0.7, with optimized wave parameters.

2) OKCD + BC

We now consider the case of OKCD, where the current is generated by the Ohkawa effect; that is, a sink of electrons with negative $p_{//}$ under the trapped/passing boundary that results from the wave induced trapping. The plasma parameters are again those of Alcator C-Mod at $\rho$=0.7, and the wave parameters ($N_{//}$=-0.30, $2\Omega/\omega$=0.98) are such as to optimize the OK driven current density[11] for an incident power of $P_{EC}$=10 MW. The wave-particle interaction is chosen to be located on the low-field side ($\theta$=0°), where the fraction of trapped particles is maximum, so as to maximize the OK driven current.[11] In Figure 7 are displayed contour plots of both $f_1$ and $f_{1M}$, in order to visualize the effect of (OKCD) EC quasilinear diffusion on the bootstrap distribution. The green dashed lines are contour plots of the EC diffusion coefficient. Again, we do not describe the effect on the inverted central part of the distribution $f_1$ ($p$<1.5$p_{Te}$) as its contribution to the current is negligible.

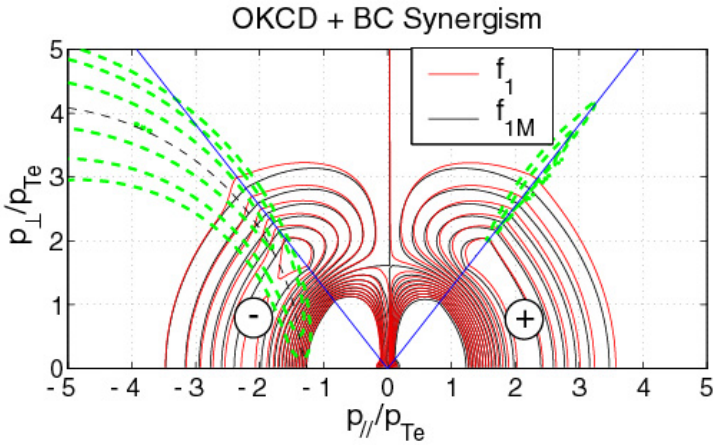


**Figure 7**: Bootstrap distribution unperturbed (black) and perturbed (red) by OKCD. The QL diffusion coefficient is represented by green dashed contours. The black dashed line is the resonance curve.

The perturbation $f_{1M}$, due to radial drifts, is negative on the $p_{//}$<0 side (minus sign on Figure 7) and therefore reduces OKCD because there are fewer electrons available for wave-induced trapping. However, the Fisch-Boozer effect on the $p_{//}$<0 side, which drives an opposite current, is also reduced because the perturbation $f_{1M}$ is negative there. Moreover, because of the antisymmetry of $f_1$ in the trapped region, pitch angle scattering through the trapped/passing boundary on the $p_{//}$<0 side results in an increase in the number of electrons with high $p_{//}$, $p_{\perp}$ on the $p_{//}$>0 side. While the reduction of OKCD due to radial drifts implies a negative synergistic current, the reduction of the Fisch-Boozer effect on the $p_{//}$<0 side and the antisymmetry of $f_1$ in the trapped region drive a positive synergistic current. The resulting synergism can be either positive or negative. In the case computed here, the synergism is positive (Table 3) and reaches 3% of OK driven current. It is interesting to note that the density of power absorbed is smaller when the effect of radial drifts is included, which can be explained by the reduced Ohkawa effect due to a smaller amount of available electrons. As a consequence, the synergism on the figure of merit reaches 4%.

| OKCD | BC | OK | OK+SYN | SYN |
|---|---|---|---|---|
| $J_{//}$ (MA/m$^2$) | 2.3 | 10.99 | 11.35 | 3% |
| $P_{abs}$ (MW/m$^3$) | - | 266.1 | 263.3 | -1% |
| $\eta$ (Am/W) | - | 0.0413 | 0.0431 | 4% |

**Table 3**: Results of the OKCD+BC computation for Alcator C-Mod parameters at r/a=0.7, with optimized wave parameters.

### *C. Effect of Wave Parameters on the Synergism*

The description of the mechanisms for ECCD+BC and OKCD+BC synergism was made using the wave parameters which gave the maximum amount of RF driven current. However, while $N_{//}$ remains essentially constant across the resonance region, the parameter $2\Omega/\omega$ varies continuously along the ray path and affects strongly RFCD, as the diffusion region in momentum space is modified along the propagation. It is therefore important to know how the synergistic current varies with the wave parameters. This is computed and shown on Figure 8 for ECCD (a) and OKCD (b).

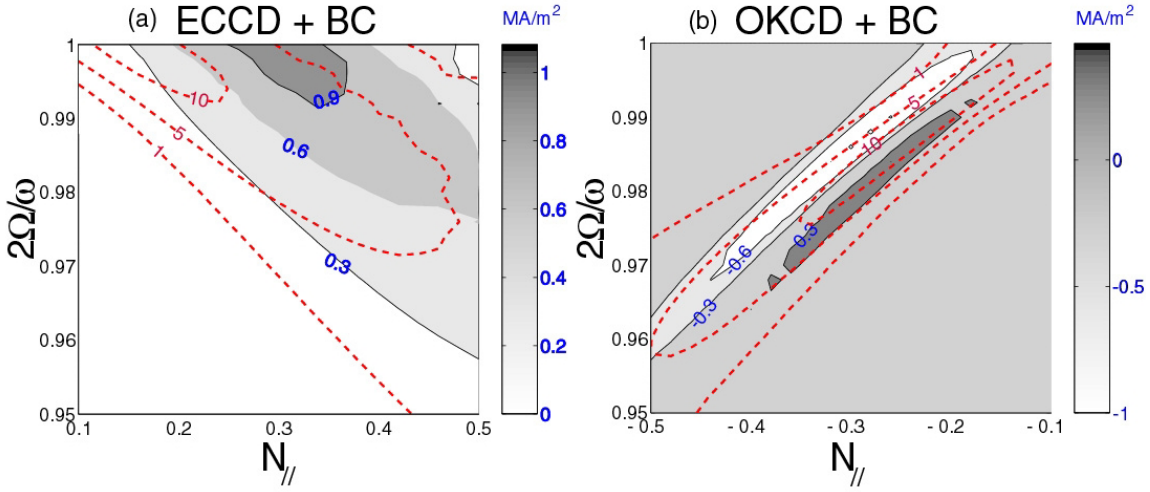


**Figure 8**: RF driven current (red dashed contours) and synergistic current (black filled contours) for (a) ECCD+BC, and (b) OKCD+BC.

Concerning ECCD+BC, we observe that the peak in synergistic current does not coincide with the peak in EC driven current. The synergistic current is maximum when the diffusion region in momentum space starts to overlap with the bulk of untrapped electrons; at this position, the synergistic current can represent more than 20% of the EC driven current. As $2\Omega/\omega$ becomes closer to 1, the pitch angle scattering due to the presence of trapped electrons is enhanced (the diffusion region in momentum space and the trapped region are closer), which reduces ECCD but increases the synergism, as described in Section B.1.

In the case of OKCD + BC, we know from Section B.2 that the synergism results from the opposition of a negative Ohkawa effect and a positive Fisch-Boozer effect. While $2\Omega/\omega$ remains far from 1, the diffusion region in momentum space is far from the trapped region and the Fisch-Boozer effect dominates. The resulting synergism is positive. However, as the quasilinear diffusion region approaches the trapped region, the negative Ohkawa effect on the synergism starts to dominate, leading to an anti-synergism. These considerations are in agreement with the results on Figure 8.

### *D. Conclusions*

The synergism between ECCD or OKCD and the bootstrap current is described at a kinetic level, using an expansion of the distribution function that is computed numerically with the code DKE. It appears that the synergism between ECCD and BC is always positive, while it can be either positive or negative for OKCD+BC, depending on how far from the trapped region the wave-particle interaction occurs. In future work, the synergism will be evaluated on a global scale, including the evolution of the wave characteristics (including the wave power) along the propagation. From the results of Section C, it can already be predicted that in the case of Alcator C-Mod, the global synergism will be less that 10% for ECCD+BC, and even lower for OKCD+BC.

## 3. Coherent Acceleration of Ions by Electrostatic Waves in a Magnetic Field

**Sponsors**
Department of Energy (DoE)/National Science Foundation (NSF) Contract DE-FG02-99ER-54555

**Project Staff**
D. J. Strozzi, A. K. Ram, A. Bers

The motion of charged particles in the presence of electrostatic waves is a rich dynamical system with important physical applications in laboratory fusion experiments (such as plasma heating and current drive) and space physics (such as ion energization in the ionosphere). Our group has been studying ways in which ion heating can be enhanced in the presence of multiple, as opposed to single, waves. We report here on a coherent energization process that occurs when two waves interact with ions in the presence of a uniform magnetic field $\vec{B}$. This is a generalization of earlier work in this group[15,16] on waves propagating perpendicularly to $\vec{B}$, to include finite projections of the wavenumbers along $\vec{B}$. Results of this work have been submitted for publication to the journal *Physics of Plasmas;* [17] preliminary results were presented earlier.[2] We find that coherent energization occurs when the Doppler-shifted wave frequencies differ by nearly an integer multiple of the ion cyclotron frequency $\omega_{ci} = qB_0 / M$. Furthermore, as the magnitude of the difference between the parallel wavenumbers of the two waves increases from zero the coherent acceleration is limited.

The equation of motion for an ion in a magnetic field $\vec{B} = B_0\hat{z}$ interacting with two electrostatic waves is

$$M\ddot{\vec{x}} = q\vec{v}\times\vec{B} + \sum_{i=1}^{2}\Phi_i\vec{k}_i\sin(\vec{k}_i\cdot\vec{x} - \omega_i t) \tag{8}$$

We assume the two waves propagate in the x-z plane (an angle between the components of $\vec{k}_1$ and $\vec{k}_2$ perpendicular to $\vec{B}$ limits the coherent energization[18]). The Hamiltonian for this system is

$$H(\phi, z, I, v_z, t) = I + \frac{1}{2}v_z^{\,2} + \sum_{i=1}^{2}\varepsilon_i\cos(k_{ix}\rho\sin\phi + k_{iz}z - \nu_i t) \tag{9}$$

We have used nondimensional variables where length is scaled to $1/k_{1x}$ and time to $1/\omega_{ci}$. $\varepsilon_i = qk_{1x}^2\Phi_i/M\omega_{ci}^2$ measures the normalized amplitude of the $i^{th}$ wave, $\nu_i = \omega_i/\omega_{ci}$, $I = (v_x^2 + v_y^2)/2$ is the ion gyro-action, $\rho = (2I)^{1/2}$ is the ion gyroradius, and $\Phi = \arctan(-v_y/v_x)$ is the gyrophase.

For any choice of $\nu_i$, there is a region in phase space with a lower bound of $\rho \approx \min(\nu_i)$ in which the ion motion is stochastic.[18, 19] In addition, coherent acceleration occurs when a resonance condition between the two waves holds, namely when

$$\nu_1 - \nu_2 - (k_{1z} - k_{2z})v_z \equiv N \in Z \tag{10}$$

---

[15] A. K. Ram, D. Bénisti, and A. Bers, "Ionospheric Ion Acceleration by Multiple Electrostatic Waves," *J. Geophys. Res.* 103(A5): 9431-40 (1998).
[16] D. Bénisti, A. K. Ram, and A. Bers, "Ion Dynamics in Multiple Electrostatic Waves in a Magnetized Plasma – Part I: Coherent Acceleration," *Phys. Plasmas* 5(9): 3224-32 (1998).
[17] D. J. Strozzi, A. K. Ram, and A. Bers, "Coherent Acceleration of Magnetized Ions by Electrostatic Waves With Arbitrary Wavenumbers," submitted to *Phys. Plasmas* (February 2003).
[18] A. K. Ram, L. Kang, and A. Bers, "Plasma Wave Interactions—RF Heating and Current Generation: Section 1.1.3 – Energization of Ions by Two Lower Hybrid Waves," *Progress Report No. 141,* MIT Research Laboratory of Electronics, Cambridge, 1999, pp. 234–236.
[19] C. F. F. Karney and A. Bers, "Stochastic Ion Heating by a Perpendicularly Propagating Electrostatic Wave," *Phys. Rev. Lett.* 39(9): 550-54 (1977).

is an integer. For single or multiple waves with $\nu_i$ an integer, stochastic "webs" form in phase space.[20, 21] Here we do not wish to study this effect, so we assume that no $\nu_i$ is an integer. Figure 9(a) shows the coherent motion of ions from low to high energies when the wave frequencies differ by an integer. Figure 9(b) shows that this effect disappears when the frequency difference is not an integer.

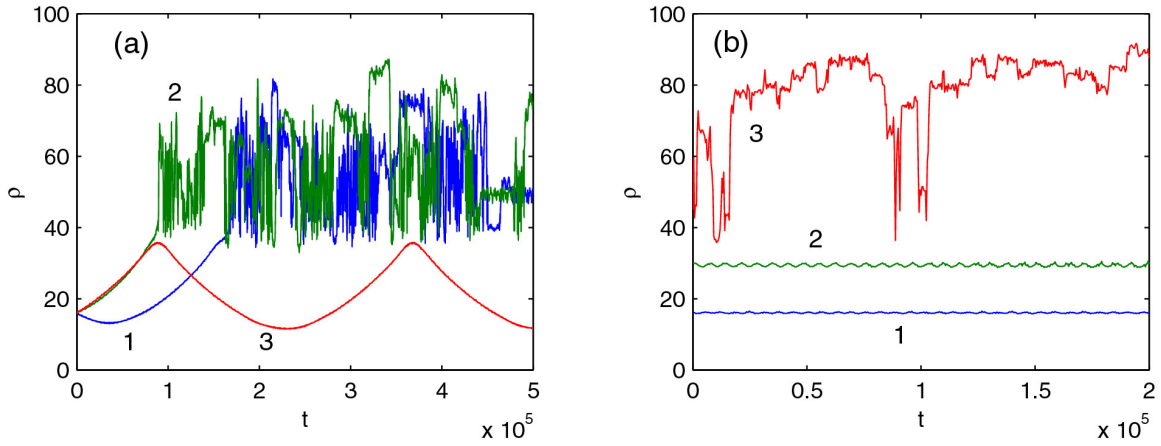


**Figure 9**: $\rho$ versus t for two perpendicularly-propagating waves using the full Hamiltonian H in Eq. (9). The wave parameters are $\varepsilon_i$=4, $k_{ix}$=1, $k_{iz}$=0, $\nu_1$=40.37, and $\nu_2$=39.37 for (a) and 39.369 for (b). The initial conditions are $\phi_0$=(-0.3,0.2,0.4)$\pi$, (a) $\rho_0$=15.95 ($\xi_0 \equiv \rho_0/\nu_1$=0.4) for all ions and (b) $\rho_0$=15.95,30,45 for ions 1, 2, and 3, respectively.

We can analyze the coherent motion using the Lie transformation perturbation theory.[22] Upon carrying out the perturbation analysis to second order in the field amplitudes $\varepsilon_i$, we obtain an approximate Hamiltonian which describes the coherent motion. The Lie method gives a new Hamiltonian $\overline{H}$ that governs the dynamics of new variables $\bar{x}$. The evolution of the old variables x is described by the original Hamiltonian H (x and $\bar{x}$ are vectors of all the new and old variables). $\overline{H}$ just describes the coherent motion of x, and the change of variables from x to $\bar{x}$ accounts for the small, rapid fluctuations. This description only applies for the coherent motion and breaks down when the motion of the ions becomes chaotic.

The full Hamiltonian H is split into an unperturbed, or slowly-varying, $H_0$ and a perturbing, or rapidly varying, $H_1$:

$$H_0 = I + \frac{1}{2} v_z^{\,2}, \qquad H_1 = \sum_{i=1}^{2} \varepsilon_i \cos(k_{ix}\rho \sin\phi + k_{iz} z - \nu_i t) \tag{11}$$

$\overline{H}$ is found by expanding it in powers of the perturbation parameter $\varepsilon$ (we order $\varepsilon \sim \varepsilon_1 \sim \varepsilon_2$): $\overline{H} = \overline{H}_0 + \overline{H}_1 + \overline{H}_2 + \ldots$. The new coordinates $\bar{x}$ are close to x, so that $\overline{H}_0 = H_0$. From the Lie method we find that as long as $\nu_i$ is not an integer, $\overline{H}_1$=0. Similarly, $\overline{H}_2$=0 unless $\nu_1$-$\nu_2$, $\nu_1$+$\nu_2$, or 2$\nu_i$ is an integer is an integer. We assume that only $\nu_1$-$\nu_2$ is an integer. This gives the Hamiltonian up to order $\varepsilon^2$:

[20] A. Fukuyama, H. Momota, R. Itatani, and T. Takizuka, "Stochastic Acceleration by an Electrostatic Wave Near Ion Cyclotron Harmonics," *Phys. Rev. Lett.* 38(13): 701-4 (1977).
[21] D. Bénisti, A. K. Ram, and A. Bers, "Ion Dynamics in Multiple Electrostatic Waves in a Magnetized Plasma – Part II: Enhancement of the Acceleration," *Phys. Plasmas* 5(9): 3233-41 (1998).
[22] J. R. Cary, "Lie Transform Perturbation Theory for Hamiltonian Systems," *Phys. Reports* 79(2): 129-59 (1981).

$$\bar{H}(\bar{\Psi},\bar{z},\bar{I},\bar{v}_z)=\frac{1}{2}\bar{v}_z^{\,2}+S_0(\bar{I},\bar{v}_z)+S_-(\bar{I},\bar{v}_z)\cos(N\bar{\psi}+\Delta k_z\bar{z}) \tag{12}$$

which describes the coherent motion. Here $\Psi=\phi-t$ and $\Delta k_z=k_{1z}-k_{2z}$. $S_0$ and $S_-$ are complicated functions that, importantly, depend only on $\bar{I}$ and $\bar{v}_z$. In the limit $\nu_i>>1$, $S_0,S_-\sim\varepsilon^2/\nu_1^2$.

The coherent dynamics given by $\bar{H}$ has two constants of the motion, $\bar{H}$ and $\bar{v}_z-(\Delta k_z/N)\bar{I}$ where $\Delta k_z=k_{1z}-k_{2z}$. Thus, the coherent system is completely integrable and contains no stochastic dynamics even though it has two degrees of freedom. The second constant relates the coherent z motion to the perpendicular motion:

$$\bar{v}_z(\bar{I})=\bar{v}_{z0}+\frac{\Delta k_z}{N}(\bar{I}-\bar{I}_0) \tag{13}$$

Here the subscript zero refers to a quantity's initial value. Since $\bar{v}_z$ is a function of $\bar{I}$, $S_0$ and $S_-$ are just functions of $\bar{I}$. We can therefore bound the accessible region of phase space with the potential barriers $H_+$ and $H_-$:

$$H_-\le\bar{H}\le H_+,\qquad H_\pm(\bar{I})=\frac{1}{2}\bar{v}_z^{\,2}(\bar{I})+S_0(\bar{I})\pm|S_-(\bar{I})| \tag{14}$$

Since $\bar{H}$ is a constant of the motion, an ion oscillates between the points where $H_-(\bar{I})=\bar{H}$ or $H_+(\bar{I})=\bar{H}$.

Figure 10 shows the potential barriers $H_\pm$ versus $\bar{\rho}$ for the parameters of Figure 9 (a). Also the values of $\bar{H}$ for the three initial conditions of Figure 9 (a) are plotted. The turning points predicted by the potential barriers agree well with those obtained from the numerical integration of (8).

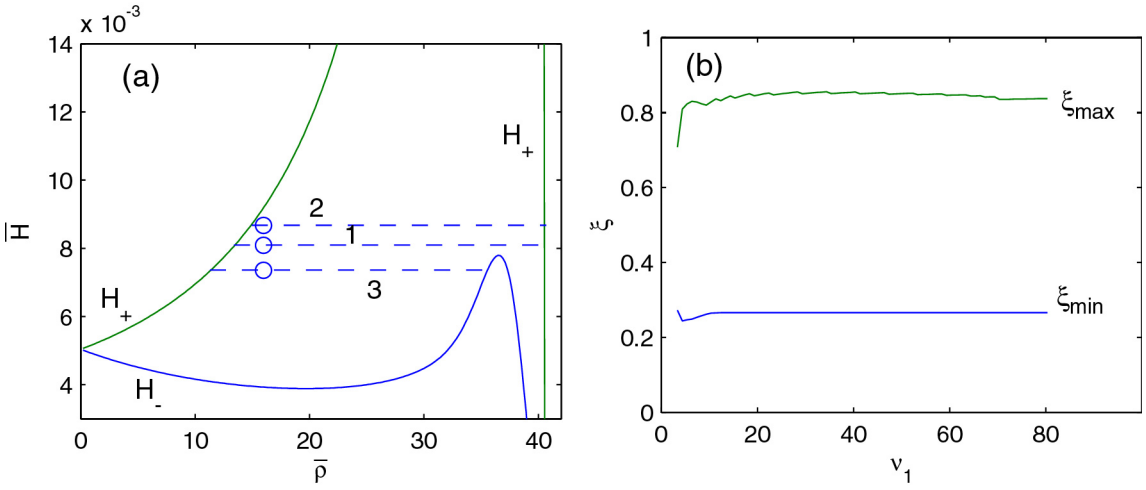


**Figure 10**: (a) $H_+$ and $H_-$ versus. $\bar{\rho}$ for the parameters of Figure 9(a). The values of $\bar{H}$ for the three initial conditions of Figure 9(a) are also indicated. (b) Average $\xi_{min}$ and $\xi_{max}$ versus $\nu_1$ for waves with $k_{ix}=1,k_{iz}=0$, $\varepsilon_1=\varepsilon_2$ are equal but otherwise arbitrary, and $\nu_2=\nu_1-1$. $\xi_0=0.4$, and the average is over $\phi_0=(0,0.05,\ldots,1)\pi$.

The perturbation analysis determines the dependence of the ion motion on wave parameters. We find that the range of coherent motion in $\rho$ scales linearly with the wave frequencies. As the wave frequencies are varied (but their difference kept constant), the minimum and maximum $\xi_{min}$ and $\xi_{max}$ (where $\xi\equiv\rho/\nu_1$) is roughly the same for ions with the same initial $\xi_0$. For two perpendicularly-propagating waves ($k_{iz}=0$) we

can neglect the z motion. $\overline{H}$ scales like $\varepsilon^2$, so that the period of coherent oscillation $\tau$ is proportional to $\varepsilon^{-2}$. Furthermore, from the asymptotic scalings of $S_0$ and $S_-$, we can infer that $\tau \sim \nu_1^4/\varepsilon^2$. In Figure 11 we compare this analytical scaling with that obtained from numerical solution of the equations of motion generated by $\overline{H}$.

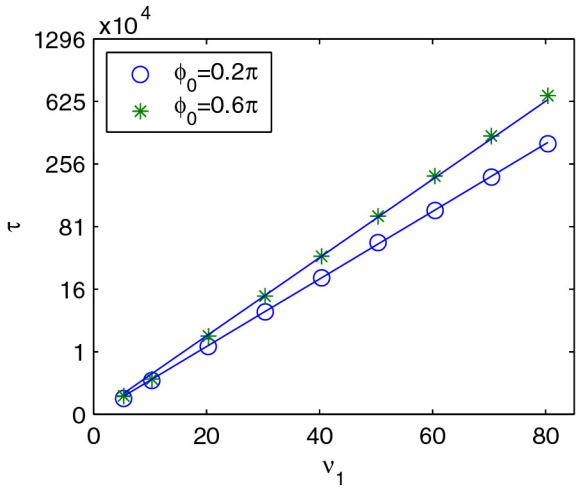


**Figure 11**: Period of coherent oscillation versus $\nu_1$. The other wave parameters are the same as in Figure 9(a). The initial conditions are $\xi_0$=0.4 and $\phi_0$=(0.2,0.6)$\pi$. The discrete points are the observed periods from integrations of the dynamics given by $\overline{H}$. The solid lines are $A\nu_1^4$ with A chosen to match the observed period at $\nu_1$=40.37. The vertical axis is scaled so that $\nu_1^4$ is a straight line.

For obliquely-propagating waves ($k_{iz}\neq 0$) the coherent motion is drastically different when $k_{1z}=k_{2z}$ as opposed to when $k_{1z} \neq k_{2z}$. For the case $k_{1z}=k_{2z}$, the resonance condition is simply that $\nu_1-\nu_2$ is an integer, and is satisfied by all ions regardless of their initial conditions. Eq. (13) predicts that there will be no coherent motion in $v_z$, only small incoherent fluctuations. Figure 12 shows the coherent motion in $\rho$ and the stochastic region in both $\rho$ and $v_z$ for two waves with $k_{1z}=k_{2z}$ and propagating at 45° with respect to $\vec{B}$.

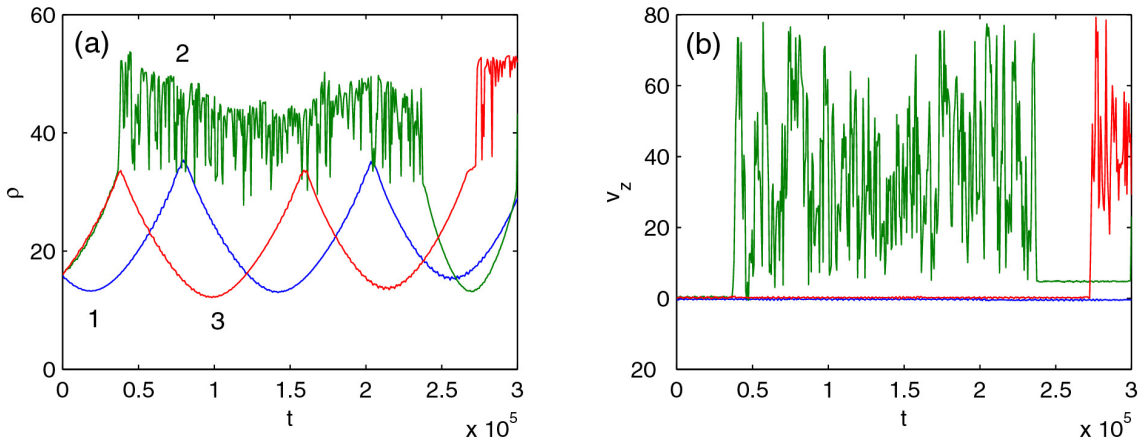


**Figure 12**: (a) $\rho$ versus t and (b) $v_z$ versus t for the same parameters as in Figure 9(a), except that $k_{1z}=k_{2z}=1$.

The coherent energization for $k_{1z}=k_{2z}$ is quite similar to the case of perpendicularly propagating ($k_{iz}=0$) waves. The major difference is that the bump in $H_-$ [near $\bar{\rho}=0$ in Figure 10(a)] becomes higher and reflects more low-energy ions as $k_{1z}$ is increased. The lowering of the average energy gained by a group of ions with the same initial $\rho_0$ but different $\phi_0$ is shown in Figure 13, and is small.

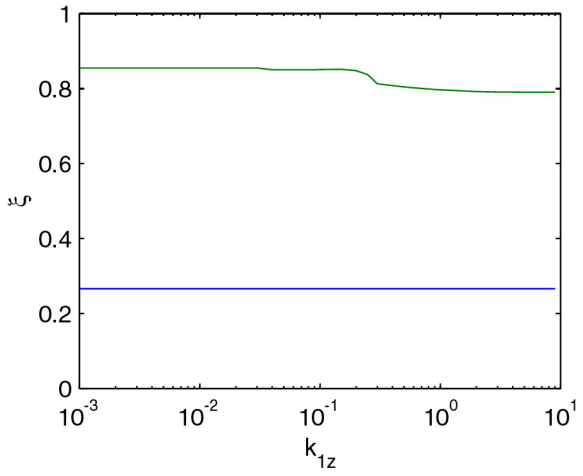


**Figure 13**: Average $\xi_{min}$ and $\xi_{max}$ versus $k_{1z}$ for $k_{1z}=k_{2z}$ based on the bounds $H_{\pm}$. Here $\nu_1$=40.37,N=1, and $k_{1x}=k_{2x}=0$. The average is over ions with $\xi_0$=0.4 and $\phi_0$=(0,0.05,...,1)$\pi$..

For unequal parallel wavenumbers, the coherent motion is over a smaller range in $\rho$. Eq. (13) predicts that $v_z$ undergoes coherent acceleration for differing parallel wavenumbers. The term $v_z^2/2$ in $\bar{H}$ is no longer a constant and strongly modifies the potential barriers $H_{\pm}$. We see the coherent motion in $v_z$, and the dominant effect of $v_z^2/2$ on $H_{\pm}$ in Figure 14.

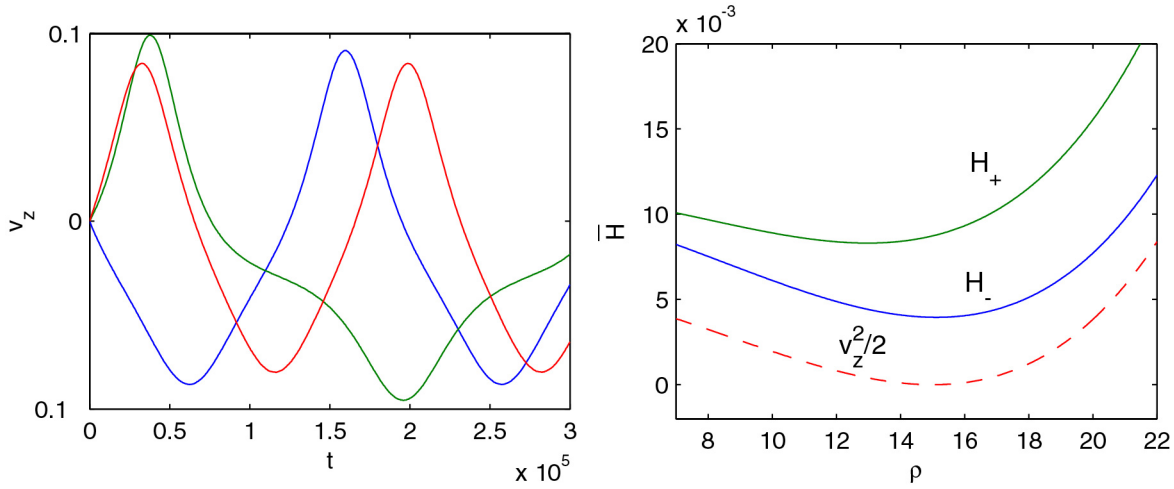


**Figure 14**: (a) $v_z$ versus t and (b) $H_{\pm}$ versus $\rho$ for the same parameters as Figure 9(a) except that $k_{1z}$=0.001 and $k_{2z}$=0.

Since the condition (10) depends on $v_z$, it is clear that ions in resonance will not remain so for all time. A difference between the parallel wavenumbers is similar to $\nu_1$-$\nu_2$ not being an integer. For $\nu_1=\nu_2+N+\Delta\nu$, the coherent Hamiltonian is

$$\overline{H}_{off} = -\frac{\Delta\nu}{N}\bar{I} + \overline{H} \tag{15}$$

There is a small range around $\Delta k_z=0$ and $\Delta\nu=0$ for which there is coherent acceleration. From the asymptotic form of $S_0,S_-\sim 1/\nu_1^2$, we estimate how this range depends on the wave frequencies. Let $\xi_a$ be the upper (or lower) bound of coherent motion in $\xi$ for frequencies $\nu_{1a}$ and $\nu_{2a}=\nu_{1a}-N$. Then for two different frequencies $\nu_{1b}$ and $\nu_{2b}=\nu_{1b}-N$, we should approximately have

$$\xi_b(\Delta k_z) \approx \xi_a\left(\left(\frac{\nu_{1b}}{\nu_{1a}}\right)^3 \Delta k_z\right) \tag{16}$$

Suppose $\xi_a$ is large for $k_1<\Delta k_z<k_2$, and that $\nu_{1b}=4\nu_{1a}$. Then $\xi_b$ is large only for $k_1/64<\Delta k_z<k_2/64$. Coherent motion occurs over a smaller range of $\Delta k_z$ when the wave frequencies are larger. Similarly,

$$\xi_b(\Delta\nu) \approx \xi_a\left(\left(\frac{\nu_{1b}}{\nu_{1a}}\right)^4 \Delta\nu\right) \tag{17}$$

Figure 15 demonstrates that these scalings are fairly accurate.

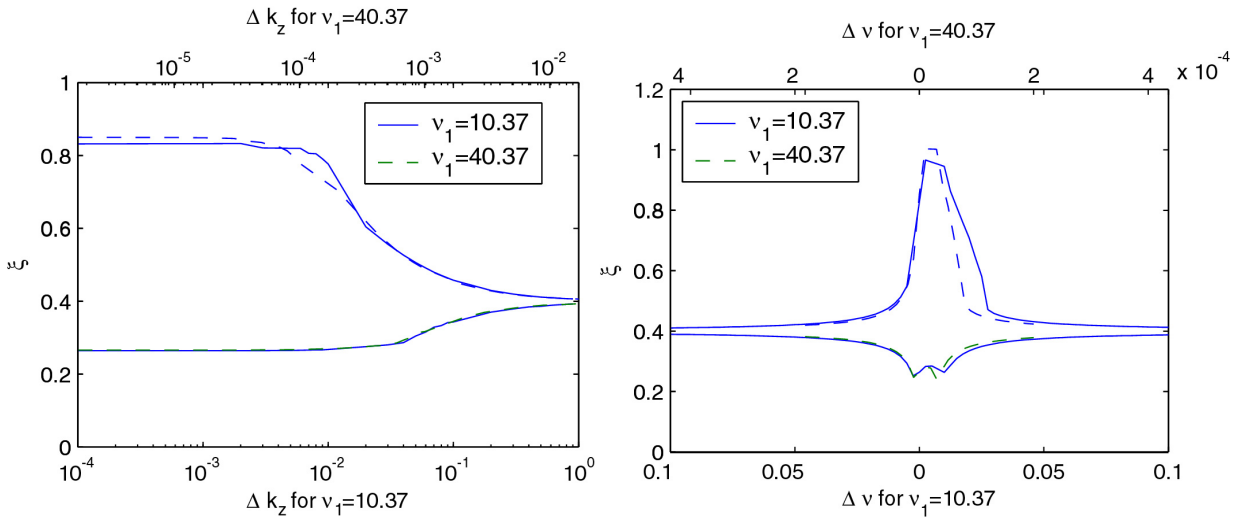


**Figure 15**: Average $\xi_{min}$ and $\xi_{max}$ versus (a) $\Delta k_z$ and (b) $\Delta\nu$ from $H_\pm$ for $\nu_2=\nu_1-1-\Delta\nu$, $\nu_1=10.37$ (solid) or 40.37 (dashed) and the other wave parameters as in Figure 9. Initial conditions and averaging are as in Figure 12. The abscissa for $\nu_1=40.37$ has been rescaled by $(10.37/40.37)^3$ and $(10.37/40.37)^4$, respectively. If the scalings in (16) and (17) were exact, the solid and dashed lines would coincide.

## 4. Interaction of Ions With Localized Fields

**Sponsors**
Department of Energy (DoE)/National Science Foundation (NSF) Contract DE-FG02-99ER-54555 and National Science Foundation (NSF) Contract ATM 98-06328.

**Project Staff**
Dr. A. K. Ram and Professor A. Bers

There are physical situations where the interaction of charged particles takes place with fields that are spatially localized. This happens, for instance, in space plasmas where the fields are localized to density gradients within density cavities.[23] The observed fields are electrostatic, essentially perpendicular to the magnetic field, and localized over spatial distances that are small compared to the ion Larmor radius. The interaction of ions with such localized field structures is different from that with a plane wave or a set of plane waves.[15,16,21] The primary difference is that the interaction of ions with the fields occurs over only a small fraction of the ion orbit.

Let us consider the situation in which the wave fields are localized radially in a cylindrical cavity aligned along a magnetic field. This represents, for example, lower hybrid density cavities in the auroral ionosphere.[24] We assume that the wave fields are radial and we look at the ion motion in a plane perpendicular to a uniform magnetic field $\vec{B} = B_0\hat{z}$. In cylindrical coordinates, the equations of motion are

$$\frac{dr}{dt} = \mathrm{v}_r \tag{18}$$

$$\frac{d\theta}{dt} = \frac{\mathrm{v}_\theta}{r} \tag{19}$$

$$\frac{d\mathrm{v}_r}{dt} = \mathrm{v}_\theta\left(\Omega + \frac{\mathrm{v}_\theta}{r}\right) + \frac{QE_r}{M} \tag{20}$$

$$\frac{d\mathrm{v}_\theta}{dt} = -\mathrm{v}_r\left(\Omega + \frac{\mathrm{v}_\theta}{r}\right) \tag{21}$$

where $\Omega = QB_0/M$ is the angular ion cyclotron frequency, and $Q$ and $M$ are the charge and mass of the ion, respectively. We assume the following form of a spatially localized electric field that tries to model the resonant electrostatic fields in density gradients:[23,25]

[23] K. L. McAdams, J. LaBelle, P. W. Schuck, and P. M. Kintner, "PHAZE II Observations of Lower Hybrid Burst Structures Occurring on Density Gradients," *Geophys. Res. Lett.* 25(16): 3091-4 (1998).
[24] S. H. Høymork, H. L. Pécseli, B. Lybekk, J. Trulsen, and A. Eriksson, "Cavitation of Lower Hybrid Waves in the Earth's Ionosphere: A Model Analysis," *J. Geophys. Res.* 105(A8): 18519-35 (2000).
[25] A. K. Ram, D. J. Strozzi, and A. Bers, "Nonlinear Energization of Ionospheric Ions by Electrostatic Fields," *Eos (2002 American Geophysical Union Fall Meeting supplement)* 83, F1228 (2002), Paper SM21B-0554.

$$E_r = E_0\, e^{-\beta(r-a)^2} \sum_n \sin\,(k_n r + m_n \theta - \omega_n t + \phi_n) \tag{22}$$

Here $a$ is the radius of the cavity, $E_0$ is the electric field amplitude, $\beta$ determines the radial width of the field, and $k_n$, $m_n$, $\omega_n$, and $\phi_n$ are the radial wave vector, azimuthal mode number, frequency, and phase, respectively, of the $n$-th component. The equations of motion can be integrated numerically to determine the effect of the localized fields on the ion orbits.

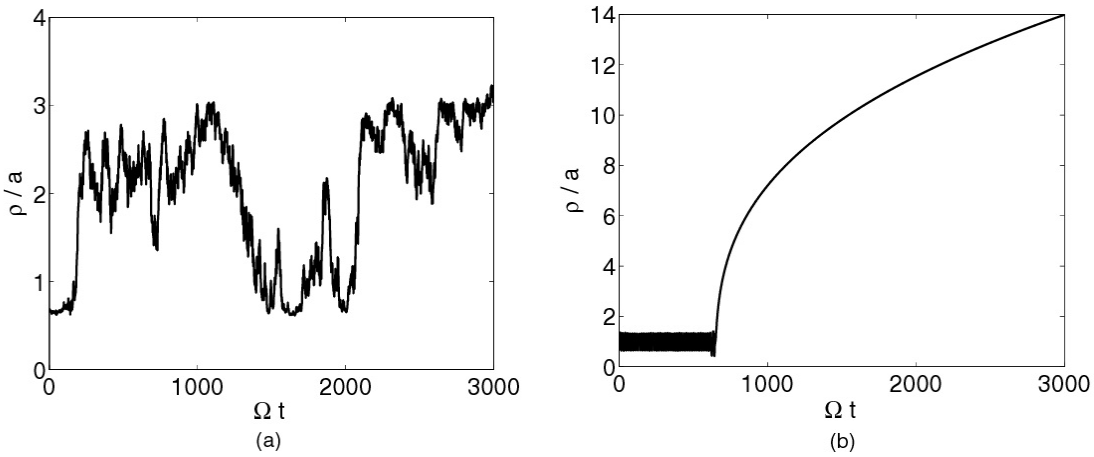


**Figure 16**: Normalized Larmor radius as a function of normalized time for (a) $\nu_1$ = 145.74, $\nu_2$ = 146.74, and (b) $\nu_1$ = 1, $\nu_2$ = 2.

Preliminary analytical analysis shows that we require $\sqrt{\beta} >> k_n$ for ion energization to occur. For illustrative purposes we choose $n$ = 2, $k_n$= 0, $\phi_n$ = 0, $m_n$ = 0, $a$ = 10 m, $\sqrt{\beta a^2} = 6.25\times10^3$, $B_0$ = 0.36 Gauss, and $E_0$ = 100 mV/m. These parameters correspond to the plasma and fields observed in the upper ionosphere.[26,27] For an ambient temperature of 0.33 eV, the initial Larmor radii of the oxygen and hydrogen ions are, respectively: $\rho_{O^+} \approx 6.5$ m, $\rho_{H^+} \approx 1.6$ m. Figure 16(a) shows the temporal evolution of the normalized ion Larmor radius for $\nu_1 = \omega_1 / \Omega = 145.74$ and $\nu_2 = 146.74$. The energization of low energy ions is chaotic from the very beginning. This is unlike the case of ion interaction with coherent plane waves where the low energy ions are, initially, coherently energized before their motion becomes chaotic.[15,16,17] This high-frequency case would correspond to $O^+$ ions interacting with lower hybrid solitary structures in the upper ionosphere.[28]

Figure 16 (b) shows the temporal evolution of the normalized ion Larmor radius for $\nu_1$ = 1 and $\nu_2$ = 2. These normalized frequencies are representative of $H^+$ ions interacting with electrostatic fields. Here we note that for $\Omega t \overset{<}{\sim} 600$ the motion of the ion is chaotic and the range of energies is bounded. After this time period, the ion monotonically gains energy. This monotonic increase is neither linear in time nor

[26] P. M. Kintner, J. Vago, S. Chesney, R. L. Arnoldy, K. A. Lynch, C. J. Pollock, and T. E. Moore, "Localized Lower Hybrid Acceleration of Ionospheric Plasma," *Phys. Rev. Lett.* 68(16): 2448-51 (1992).
[27] J. L. Vago, P. M. Kintner, S. Chesney, R. L. Arnoldy, K. A. Lynch, T. E. Moore, and C. J. Pollock, "Transverse Ion Acceleration by Localized Lower Hybrid Waves in the Topside Auroral Ionosphere," *J. Geophys. Res.* 97(A11): 16935-57 (1992).
[28] K. A. Lynch, R. L. Arnoldy, P. M. Kintner, P. W. Schuck, J. W. Bonnell, and V. Coffey, "Auroral Ion Acceleration From Lower Hybrid Solitary Structures: A Summary of Sounding Rocket Observations," *J. Geophys. Res.* 104(A12): 28515-34 (1999).

quadratic in time. The monotonic increases in energy are akin to Lévy flights[29,30] that have been conjectured and studied for field-particle interactions with a different form for the fields.[31,32,33] An observable signature of Lévy flights is that the ion distribution functions will have long tails. Ion distribution functions exhibiting such tails are indeed observed.[28]

In our continuing research effort on the interaction of ions with localized fields, we will be developing further theoretical and analytical understanding of the interaction and conditions for ion energization. We will also be developing a dynamical model for the Lévy flight behavior and determine the conditions for the existence of Lévy flights. It is clear that Lévy flight dynamics is very different from the ordinary random walk dynamics of the Brownian motion, which is the crux of the quasilinear description of wave-particle interactions. Lévy flights lead to Lévy distribution functions that have long inverse-power tails. These may be important in understanding the energetic ion distribution functions observed in the upper auroral ionosphere.[28]

[29] P. Lévy, *Calcul des probabilitiés* (Paris: Gauthier-Villars), 1925; and *Théorie de l'addition des cariables aléatoires* (Paris: Gauthier-Villars), 1937.
[30] E. W. Montroll and B. J. West, in *Fluctuation Phenomena,* eds. E. W. Montroll and J. L. Lebowitz (New York: North-Holland Publ. Co.), 1979, Chapter 2.
[31] V. V. Afanasiev, R. Z. Sagdeev, and G. M. Zaslavsky, "Chaotic Jets With Multifractal Space-Time Random Walk," *Chaos* 1(2): 143-59 (1991).
[32] S. D. Schultz, A. Bers, and A. K. Ram, "Anomalous Electron Streaming Due to Waves in Tokamak Plasmas," *Proc. 10th Topical Conference on Radio Frequency Power in Plasmas,* Boston, Massachusetts, April 1–3, 1993, A.I.P. Conf. Proc. 289 (eds. M. Porkolab, J. Hosea), New York (1994), pp. 433–436.
[33] K. Kupfer, A. Bers, and A. K. Ram, "Guiding Center Stochasticity and Transport Induced by Electrostatic Waves," in *Research Trends in Physics: Nonlinear and Relativistic Effects in Plasmas,* ed. V. Stefan (New York: American Institute of Physics), 1992, pp. 670–715.

## Publications

### Journal Articles, Published

A. Bers and A. K. Ram, “Symmetries in Dissipation-Free Linear Mode Conversion,” *Phys. Lett. A* 301 (5-6): 442-5 (2002).

A. K. Ram, A. Bers, and C. N. Lashmore-Davies, “Emission of Electron Bernstein Waves in Plasmas," *Phys. Plasmas* 9(2): 409-18 (2002).

### Journal Articles, Submitted for Publication

A. K. Ram and A. Bers, “Excitation and Emission of Electron Cyclotron Waves in Spherical Tori,” submitted to *Nucl. Fusion*.

A. Salcedo, R. J. Focia, A. K. Ram, and A. Bers, “Studies of Stimulated Raman Scattering in Laser Plasma Interactions,” submitted to *Nucl. Fusion*.

D. J. Strozzi, A. K. Ram, and A. Bers, “Coherent Acceleration of Magnetized Ions by Electrostatic Waves With Arbitrary Wavenumbers," submitted to *Phys. Plasmas*.

### Meeting Papers, Published

A. Bers and A. K. Ram, “Symmetries in Dissipation-Free Linear Mode Conversions,” *Proc. International Sherwood Fusion Theory Meeting,* Rochester, New York, April 22–24, 2002, Paper 1D37.

D. J. Strozzi, A. K. Ram, and A. Bers, “Coherent and Stochastic Motion of Magnetized Ions by Oblique Electrostatic Waves,” *Proc. International Sherwood Fusion Theory Meeting,* Rochester, New York, April 22–24, 2002, Paper 2C48.

A. Bers and A. K. Ram, “General Proof of Symmetry Relations in Mode Conversion With Application to, Excitation of, and Emission From, Electron Bernstein Waves,” invited, *Proc. 12th Joint Workshop on Electron Cyclotron Emission and Electron Cyclotron Resonance Heating,* Aix-en-Provence, France, May 13–16, 2002, to be published by World Scientific (Singapore), pp. 125–130, also <http://wshop.free.fr/ec12/PAPERS/093-Bers.pdf>.

J. Decker, Y.Peysson, A. Bers, and A. K. Ram, “Self-Consistent ECCD Calculations With Bootstrap Current,” *Proc. 12th Joint Workshop on Electron Cyclotron Emission and Electron Cyclotron Resonance Heating,* Aix-en-Provence, France, May 13–16, 2002, to be published by World Scientific (Singapore), pp. 113–118, also <http://wshop.free.fr/ec12/PAPERS/084-Peysson.pdf>.

A. K. Ram and A. Bers, “Electron Cyclotron Resonance Heating of Plasmas in Spherical Tori,” invited, *Proc. 12th Joint Workshop on Electron Cyclotron Emission and Electron Cyclotron Resonance Heating,* Aix-en-Provence, France, May 13–16, 2002, to be published by World Scientific (Singapore), pp. 131–136, also <http://wshop.free.fr/ec12/PAPERS/095-Ram.pdf>.

G. Taylor, P. C. Efthimion, B. Jones, T. Munsat, J. C. Hosea, R. Kaita, R. Majeski, J. Spaleta, J. R. Wilson, J. B. Wilgen, G. L. Bell, D. A. Rasmussen, A. K. Ram, A. Bers, R. W. Harvey, and A. P. Smirnov, “Mode-Converted Electron Bernstein Wave Emission Research on CDX-U and NSTX,” *Proc. 12th Joint Workshop on Electron Cyclotron Emission and Electron Cyclotron Resonance Heating,* Aix-en-Provence, France, May 13–16, 2002, to be published by World Scientific (Singapore), pp. 151–160, also <http://wshop.free.fr/ec12/PAPERS/004-Taylor.pdf>.

A. Bers and A. K. Ram, "Symmetries in Dissipation-Free Linear Mode Conversion," *Proc. 29th European Physical Society (EPS) Conference on Plasma Physics and Controlled Fusion,* Montreux, Switzerland, June 17–21, 2002, Europhysics Conference Abstracts (ECA) Vol. 26B, 2002 (eds. R. Behn and C. Varandas; CD-ROM producer B. P. Duval), Paper O-4.06. <http://crppwww.epfl.ch/eps2002/>.

J. Decker, Y. Peysson, A. Bers, and A. K. Ram, "On Synergism Between Bootstrap and Radio-Frequency Driven Currents," *Proc. 29th European Physical Society (EPS) Conference on Plasma Physics and Controlled Fusion,* Montreux, Switzerland, June 17–21, 2002, Europhysics Conference Abstracts (ECA) Vol. 26B, 2002 (eds. R. Behn and C. Varandas; CD-ROM producer B. P. Duval), Paper O-1.05. <http://crppwww.epfl.ch/eps2002/>.

A. K. Ram, A. Bers, and C. N. Lashmore-Davies, "Electron Bernstein Waves in Spherical Tori," *Proc. 29th European Physical Society (EPS) Conference on Plasma Physics and Controlled Fusion,* Montreux, Switzerland, June 17–21, 2002, Europhysics Conference Abstracts (ECA) Vol. 26B, 2002 (eds. R. Behn and C. Varandas; CD-ROM producer B. P. Duval), Paper P-5.075. <http://crppwww.epfl.ch/eps2002/>.

A. Salcedo, R. J. Focia, A. K. Ram, and A. Bers, "Studies of Stimulated Raman Scattering in Laser Plasma Interactions," to appear in *Proc. 19th International Atomic Energy Agency (IAEA) Fusion Energy Conference,* Lyon, France, October 14–19, 2002. <http://www.iaea.org/programmes/ripc/physics/>.

J. Decker, Y. Peysson, A. Bers, and A. K. Ram, "Self-Consistent RFCD and Bootstrap Current," *Bull. Am. Phys. Soc.* 47: 45 (2002).

B. Jones, G. Taylor, P. C. Efthimion, T. Munsat, V. A. Soukhanovskii, A. K. Ram, A. Bers, and R. W. Harvey, "Electron Bernstein Wave (EBW) Emission, Heating and Current Drive Research in CDX-U and NSTX," *Bull. Am. Phys. Soc.* 47: 209-10 (2002).

A. K. Ram, R. A. Cairns, C. N. Lashmore-Davies, J. Decker, and A. Bers, "Current Drive by Electron Bernstein Waves," *Bull. Am. Phys. Soc.* 47: 172 (2002).

D. J. Strozzi, A. K. Ram, and A. Bers, "Coherent and Stochastic Motion of Ions in Two Oblique Electrostatic Waves," *Bull. Am. Phys. Soc.* 47: 70 (2002).

G. Taylor, P. C. Efthimion, B. M. Jones, J. R. Wilson, J. B. Wilgen, G. L. Bell, T. S. Bigelow, D. A. Rasmussen, A. K. Ram, A. Bers, and R. W. Harvey, "Status of Electron Bernstein Wave (EBW) Research on NSTX and CDX-U," *Bull. Am. Phys. Soc.* 47: 61 (2002).

A. K. Ram, D. J. Strozzi, and A. Bers, "Nonlinear Energization of Ionospheric Ions by Electrostatic Fields," *Eos (2002 American Geophysical Union Fall Meeting supplement)* 83, F1228 (2002), Paper SM21B-0554.

**Reports**

A. K. Ram and A. Bers, "Electron Cyclotron Resonance Heating of Plasmas in Spherical Tori," Plasma Science and Fusion Center Report No. PSFC/JA-02-15 (Cambridge, Massachusetts: Massachusetts Institute of Technology, 2002).

A. Bers and A. K. Ram, "General Proof of Symmetry Relations in Mode Conversion With Application to, Excitation of, and Emission From, Electron Bernstein Waves," Plasma Science and Fusion Center Report No. PSFC/JA-02-16 (Cambridge, Massachusetts: Massachusetts Institute of Technology, 2002).

A. K. Ram, A. Bers, and C. N. Lashmore-Davies, "Electron Bernstein Waves in Spherical Tori," Plasma Science and Fusion Center Report No. PSFC/JA-02-17 (Cambridge, Massachusetts: Massachusetts Institute of Technology, 2002).

A. Bers and A. K. Ram, “Symmetries in Dissipation-Free Linear Mode Conversion,” Plasma Science and Fusion Center Report No. PSFC/JA-02-18 (Cambridge, Massachusetts: Massachusetts Institute of Technology, 2002).

J. Decker, Y. Peysson, A. Bers, and A. K. Ram, “On Synergism Between Bootstrap and Radio-Frequency Driven Currents,” Plasma Science and Fusion Center Report No. PSFC/JA-02-19 (Cambridge, Massachusetts: Massachusetts Institute of Technology, 2002).

A. Bers and A. K. Ram, “Symmetries in Dissipation-Free Linear Mode Conversion, Plasma Science and Fusion Center Report No. PSFC/JA-02-20 (Cambridge, Massachusetts: Massachusetts Institute of Technology, 2002).

A. Salcedo, R. J. Focia, A. K. Ram, and A. Bers, “Studies of Stimulated Raman Scattering in Laser Plasma Interactions,” Plasma Science and Fusion Center Report No. PSFC/JA-02-21 (Cambridge, Massachusetts: Massachusetts Institute of Technology, 2002).

A. Salcedo, R. J. Focia, A. K. Ram, and A. Bers, “Studies of Stimulated Raman Scattering in Laser Plasma Interactions,” Plasma Science and Fusion Center Report No. PSFC/JA-02-24 (Cambridge, Massachusetts: Massachusetts Institute of Technology, 2002).

**Theses**

R. J. Focia, *Observation and Characterization of Single Hot Spot Laser-Plasma Interactions*, Ph.D. dissertation, Department of Electrical Engineering and Computer Science, MIT, February 2002.

A. Salcedo, *Coupled Modes Analysis of SRS Backscattering, with Langmuir Decay and Possible Cascadings,* Ph.D. dissertation, Department of Electrical Engineering and Computer Science, MIT, December, 2001.